Journal of Applied Mechanics and Technical Physics, Vol. 48, No. 1, pp. 17–26, 2007

SHOCK-WAVE-INITIATED LIFTING OF PARTICLES FROM A CAVITY

I. A. Bedarev, Yu. A. Gosteev, and A. V. Fedorov

UDC 534.222.2; 662.612.32

The dynamics of particles of the disperse phase in a turbulent gas flow in planar shock waves sliding along a solid surface with a trapezoid cavity is examined numerically. Lifting of particles from the cavity walls is calculated in the approximation of a rarefied gas suspension. It is shown that the intensity of the transient shock wave and the initial positions of particles have a significant effect on the particle-lifting properties. The height of particle lifting is found to nonmonotonically depend on the initial streamwise coordinate and shock-wave Mach number. It is shown that zones of aggregation and subtraction of particles may be formed at the cavity bottom.

Key words: *shock wave, cavity, turbulent separated flow, rarefied gas suspension, particle lifting, mathematical modeling.*

Introduction. The problem of formation of a gas suspension under shock-wave forcing of a layer of a disperse material has been considered in many papers (see [1–7]). Some activities in this field were reviewed in [1]. The model of single particles used in [2] to describe lifting of particles of a rarefied dusty layer behind a transient shock wave (SW) takes into account the Saffman force and aerodynamic interference of the particle and the substrate in equations of motion of the particle. Using this model made it possible to obtain a qualitative description of the initial stage of lifting of particles ranging from 1 to 250 μm by transient shock waves of low and moderate intensity (the SW Mach number was $\mathrm{M_{SW}} = 1.1$–2.7), based on an analytically prescribed flow field of the gas phase in the approximation of an incompressible boundary layer. It seems of interest to perform computations without the restricting assumption made in [2] on setting the law of motion of the carrier phase in analytical form and to study the problem within the framework of the single-particle mode, with the flow field being computed on the basis of the k–ω model of turbulence.

Formulation of the Problem. We consider the motion of a planar shock wave along a solid surface with a trapezoid cavity. There are particles of a disperse material on the cavity walls (and, possibly, inside the cavity as well). A sketch of the flow and flow-region geometry are shown in Fig. 1. At the initial time, the SW is on the left of the cavity at a certain distance from the point A; it propagates from left to right over a quiescent medium and reaches the cavity at a certain time. The flow arising in the vicinity of the cavity can induce separation of particles from the surface and their motion in the flow field of the gas. Let us consider the characteristics of this process by numerical methods of mathematical modeling.

Mathematical Model. *Gas Phase.* To describe the motion of the carrier phase, we used the Favre-averaged full Navier–Stokes equations written in a generalized curvilinear coordinate system $\eta = \eta(x, y)$, $\xi = \xi(x, y)$ [8]:

$$\frac{\partial \boldsymbol{U}}{\partial t} + \frac{\partial \tilde{\boldsymbol{F}}}{\partial \xi} + \frac{\partial \tilde{\boldsymbol{G}}}{\partial \eta} = 0. \tag{1}$$

Khristianovich Institute of Theoretical and Applied Mechanics, Siberian Division, Russian Academy of Sciences, Novosibirsk 630090; bedarev@itam.nsc.ru; gosteev@itam.nsc.ru; fedorov@itam.nsc.ru. Translated from Prikladnaya Mekhanika i Tekhnicheskaya Fizika, Vol. 48, No. 1, pp. 24–34, January–February, 2007. Original article submitted February 26, 2006; revision submitted March 30, 2006.

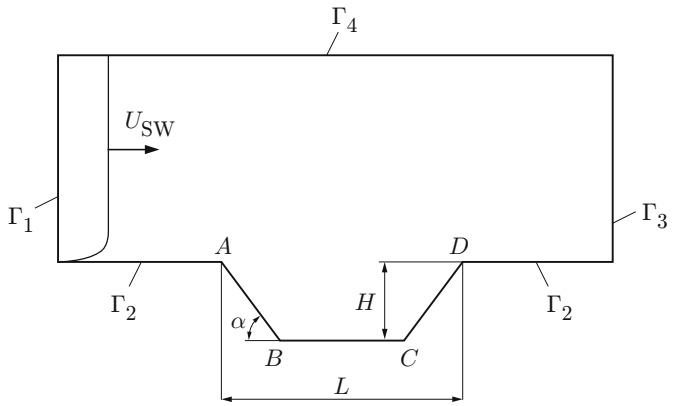

Fig. 1. Sketch of the flow.

Here $\boldsymbol{U}$ is the vector of conservative variables

$$\boldsymbol{U} = \begin{pmatrix} \rho \\ \rho u \\ \rho v \\ \rho(E+k) \end{pmatrix};$$

the fluxes $\tilde{\boldsymbol{F}}$ and $\tilde{\boldsymbol{G}}$ consist of inviscid (subscript "inv") and viscous (subscript "vis") parts

$$\tilde{\boldsymbol{F}} = \tilde{\boldsymbol{F}}_{\mathrm{inv}} - \tilde{\boldsymbol{F}}_{\mathrm{vis}}, \qquad \tilde{\boldsymbol{G}} = \tilde{\boldsymbol{G}}_{\mathrm{inv}} - \tilde{\boldsymbol{G}}_{\mathrm{vis}};$$

ρ is the density, u and v are the velocity components in the Cartesian coordinate system, $E = e + (u^2+v^2)/2$ and e are the total and internal energy, respectively, $k = (\rho+\rho')((u')^2+(v')^2)/(2\rho)$ is the turbulent kinetic energy, and ρ', u', and v' are the fluctuating components of density and streamwise and transverse velocity components, respectively.

The inviscid and viscous fluxes in the curvilinear coordinate system can be presented as

$$\tilde{\boldsymbol{F}}_{\mathrm{inv}} = J(\boldsymbol{F}_{\mathrm{inv}}\xi_x + \boldsymbol{G}_{\mathrm{inv}}\xi_y), \qquad \tilde{\boldsymbol{G}}_{\mathrm{inv}} = J(\boldsymbol{F}_{\mathrm{inv}}\eta_x + \boldsymbol{G}_{\mathrm{inv}}\eta_y),$$

$$\tilde{\boldsymbol{F}}_{\mathrm{vis}} = J(\boldsymbol{F}_{\mathrm{vis}}\xi_x + \boldsymbol{G}_{\mathrm{vis}}\xi_y), \qquad \tilde{\boldsymbol{G}}_{\mathrm{vis}} = J(\boldsymbol{F}_{\mathrm{vis}}\eta_x + \boldsymbol{G}_{\mathrm{vis}}\eta_y),$$

where $J = \xi_x\eta_y - \xi_y\eta_x$ is the Jacobian of transformation of coordinates. The vectors of the inviscid and viscous fluxes are written in the form

$$\boldsymbol{F}_{\mathrm{inv}} = \begin{pmatrix} \rho u \\ \rho u^2 + p \\ \rho uv \\ [\rho(E+k)+p]u \end{pmatrix}, \qquad \boldsymbol{G}_{\mathrm{inv}} = \begin{pmatrix} \rho v \\ \rho uv \\ \rho v^2 + p \\ [\rho(E+k)+p]v \end{pmatrix},$$

$$\boldsymbol{F}_{\mathrm{vis}} = \begin{pmatrix} 0 \\ t_{xx} + \tau_{xx} \\ t_{xy} + \tau_{xy} \\ f_x + \alpha_x \end{pmatrix}, \qquad \boldsymbol{G}_{\mathrm{vis}} = \begin{pmatrix} 0 \\ t_{xy} + \tau_{xy} \\ t_{yy} + \tau_{yy} \\ f_y + \alpha_y \end{pmatrix}. \tag{2}$$

Here t_{xx}, t_{xy}, and t_{yy} are the viscous stresses

$$t_{xx} = \mu\Big(\frac{4}{3}\frac{\partial u}{\partial x} - \frac{2}{3}\frac{\partial v}{\partial y}\Big), \quad t_{xy} = \mu\Big(\frac{\partial u}{\partial y} + \frac{\partial v}{\partial x}\Big), \quad t_{yy} = \mu\Big(\frac{4}{3}\frac{\partial v}{\partial y} - \frac{2}{3}\frac{\partial u}{\partial x}\Big);$$

p is the pressure, $\mu = (T/T_e)^{0.76}\mu_e$ is the viscosity, T is the temperature, and T_e and μ_e are the free-stream temperature and viscosity. The Reynolds stresses τ_{xx}, τ_{xy}, and τ_{yy} and the viscous fluxes of turbulent kinetic energy α_x and α_y are determined below, where the model of turbulence is described. The components of the viscous flux vectors in the total energy equation have the form

$$f_x = q_x + (t_{xx} + \tau_{xx})u + (t_{xy} + \tau_{xy})v, \qquad f_y = q_y + (t_{xy} + \tau_{xy})u + (t_{yy} + \tau_{yy})v,$$

where q_x and q_y are the heat fluxes

$$q_x = \gamma\Big(\frac{\mu}{\mathrm{Pr}_l} + \frac{\mu_t}{\mathrm{Pr}_t}\Big)\frac{\partial e}{\partial x}, \qquad q_y = \gamma\Big(\frac{\mu}{\mathrm{Pr}_l} + \frac{\mu_t}{\mathrm{Pr}_t}\Big)\frac{\partial e}{\partial y};$$

$\mathrm{Pr}_l = 0.723$ and $\mathrm{Pr}_t = 0.9$ are the laminar and turbulent Prandtl numbers, respectively, and γ is the ratio of specific heats.

Turbulent viscosity was calculated by a two-parameter k–ω model of turbulence proposed by Wilcox [8]:

$$\mu_t = \alpha^* \rho k/\omega$$

(α^* is a model constant and $\omega = \varepsilon/k$ is the specific dissipation rate of turbulent kinetic energy). The transport equations for k and ω are

$$\begin{gathered}\frac{\partial}{\partial t}(\rho k) + \frac{\partial}{\partial x}(\rho u k) + \frac{\partial}{\partial y}(\rho v k) = \frac{\partial \alpha_x}{\partial x} + \frac{\partial \alpha_y}{\partial y} + \Pi - \beta^* \rho \omega k, \\ \frac{\partial}{\partial t}(\rho \omega) + \frac{\partial}{\partial x}(\rho u \omega) + \frac{\partial}{\partial y}(\rho v \omega) = \frac{\partial \beta_x}{\partial x} + \frac{\partial \beta_y}{\partial y} + \frac{\alpha\omega}{k}\Pi - \beta \rho \omega^2.\end{gathered} \tag{3}$$

Here α_x, α_y, β_x, and β_y are the viscous fluxes of turbulent parameters

$$\alpha_x = \Big(\mu + \frac{\mu_t}{\sigma_k}\Big)\frac{\partial k}{\partial x}, \quad \alpha_y = \Big(\mu + \frac{\mu_t}{\sigma_k}\Big)\frac{\partial k}{\partial y}, \quad \beta_x = \Big(\mu + \frac{\mu_t}{\sigma_\omega}\Big)\frac{\partial \omega}{\partial x}, \quad \beta_y = \Big(\mu + \frac{\mu_t}{\sigma_\omega}\Big)\frac{\partial \omega}{\partial y},$$

$$\Pi = \mu_t S - \frac{2}{3}\rho k D, \quad S = 2\Big[\Big(\frac{\partial u}{\partial x}\Big)^2 + \Big(\frac{\partial v}{\partial y}\Big)^2\Big] - \frac{2}{3}D^2 + \Big(\frac{\partial v}{\partial x} + \frac{\partial u}{\partial y}\Big)^2, \quad D = \frac{\partial u}{\partial x} + \frac{\partial v}{\partial y},$$

α, σ_k, and σ_ω are model coefficients, and β and β^* are functions of the turbulent Mach number $\mathrm{M}_t = \sqrt{2k}/a$ ($a = \sqrt{\gamma RT}$ is the local velocity of sound and R is the gas constant):

$$\beta^*(\mathrm{M}_t) = \beta_0^*[1 + \xi^* F(\mathrm{M}_t)], \quad \beta(\mathrm{M}_t) = \beta_0 - \beta_0^* \xi^* F(\mathrm{M}_t);$$

$$F(\mathrm{M}_t) = [\mathrm{M}_t^2 - \mathrm{M}_{t0}^2]\varphi(\mathrm{M}_t - \mathrm{M}_{t0})$$

[$\varphi(\mathrm{M})$ is the Heaviside function]. The constants have the following values: $\alpha^* = 1$, $\alpha = 5/9$, $\sigma_k = 1/2$, $\sigma_\omega = 1/2$, $\beta_0 = 3/40$, $\beta_0^* = 9/100$, $\xi^* = 3/2$, and $\mathrm{M}_{t0} = 1/4$.

This system was supplemented by initial and boundary conditions. At the initial time, the distributions of the gas-phase parameters were consistent with the distributions for an inviscid normal shock wave located near the boundary Γ_1. The following conditions were set at the domain boundaries: initial conditions (subsonic or supersonic piston) on Γ_1, no-slip condition for velocity and adiabaticity for gas temperature on Γ_2, and "soft" conditions on Γ_3 and Γ_4.

The system of differential equations (1)–(3) was written in dimensionless form. The following quantities were used for scaling: characteristic length $x_* = 0.1$ m, velocity $u_* = U_{\mathrm{SW}}$ (U_{SW} is the SW velocity), time $t_* = x_*/u_*$, density $\rho_* = \rho_0$, heat capacity $c_* = c_{v,0}$, temperature $T_* = u_*^2/c_*$, and pressure and energy $p_* = e_* = u_*^2$. The quantities marked by the zero subscript refer to the quiescent state of the gas phase.

Disperse Phase. Lifting and dynamics of disperse-phase particles were computed on the basis of the known Lagrangian mathematical model used in [2, 6] to describe near-wall flows of rarefied gas suspensions. The particles are assumed to become separated from the surface under the action of the Saffman force only. The equations of motion and heat transfer for the ith particle have the form

$$\begin{gathered}m_{p,i}\frac{du_{p,i}}{dt} = f_{x,i}, \quad m_{p,i}\frac{dv_{p,i}}{dt} = f_{y,i}, \quad \frac{dx_{p,i}}{dt} = u_{p,i}, \quad \frac{dy_{p,i}}{dt} = v_{p,i}, \\ c_{2,i}m_{p,i}\frac{dT_{p,i}}{dt} = S_{p,i}k_i(T_{g,i} - T_{p,i}),\end{gathered} \tag{4}$$

where $x_{p,i}$ and $y_{p,i}$ are the coordinates, $u_{p,i}$ and $v_{p,i}$ are the longitudinal and vertical components of velocity, $T_{p,i}$ is the temperature, $c_{2,i}$ is the heat capacity, $m_{p,i} = \rho_p \pi d_{p,i}^3/6$, $d_{p,i}$, and ρ_p are the mass, diameter, and density of the

particle material, respectively, $k_i = \lambda_{g,i}\,\mathrm{Nu}_i\,/d_{p,i}$ is the heat-transfer coefficient, and Nu_i is the Nusselt number. The components of the main vector of forces acting on the particle are

$$f_{x,i} = f_{ax,i} = \frac{\pi d_{p,i}^2}{4}\,c_{D,i}\,\frac{\rho_{g,i}(u_{g,i}-u_{p,i})w_{pg,i}}{2}, \qquad f_{y,i} = f_{g,i} + f_{ay,i} + f_{\mathrm{S},i},$$

$$f_{g,i} = -m_{p,i}g, \qquad f_{ay,i} = \frac{\pi d_{p,i}^2}{4}\,c_{D,i}\,\frac{\rho_{g,i}(v_{g,i}-v_{p,i})w_{pg,i}}{2},$$

$$f_{\mathrm{S},i} = \frac{d_{p,i}^2}{4}\,c_{\mathrm{S}}\rho_{g,i}(u_{g,i}-u_{p,i})\Big(\nu_{g,i}\,\frac{\partial u}{\partial y}\,(x_{p,i},y_{p,i})\Big)^{1/2}.$$

Here $u_{g,i} = u(x_{p,i},y_{p,i},t)$, $v_{g,i} = v(x_{p,i},y_{p,i},t)$, $\rho_{g,i} = \rho(x_{p,i},y_{p,i},t)$, $\nu_{g,i} = \nu(x_{p,i},y_{p,i},t)$, and $\lambda_{g,i} = \lambda(x_{p,i},y_{p,i},t)$ are the horizontal and vertical velocity components, density, kinematic viscosity, and thermal conductivity of the gas, respectively, at the point where the particle is located, $w_{pg,i} = [(u_{g,i}-u_{p,i})^2+(v_{g,i}-v_{p,i})^2]^{1/2}$ is the particle velocity relative to the gas flow, $c_{D,i} = 24/\,\mathrm{Re}_{p,i} + 4.4/\,\mathrm{Re}_{p,i}^{0.5} + 0.42$ and c_{S} are the coefficients of the drag and Saffman forces, and $\mathrm{Re}_{p,i} = w_{pg,i}d_{p,i}/\nu_{g,i}$ is the Reynolds number of the particle. The Nusselt number Nu_i is calculated by the formula $\mathrm{Nu}_i = 2 + 0.42\sqrt{\mathrm{Re}_{p,i}}$.

Here we consider only weakly dusted flows and, hence, ignore the effect of particles on the motion of the carrier phase. The particle–wall interaction was also ignored. If a particle approached the solid wall to a distance smaller than the particle radius, it was assumed to be deposited onto the wall. The coordinates of such a particle were fixed, its velocity was assumed to vanish, and the particle was eliminated from the computational algorithm.

At the initial time, the particles were at rest:

$$t = 0\text{:} \qquad x_{p,i} = x_{p,i,0}, \quad y_{p,i} = y_{p,i,0}, \quad u_{p,i} = 0, \quad v_{p,i} = 0. \tag{5}$$

The criterion of the beginning of particle lifting (separation from the surface) was assumed to be a positive acceleration in the vertical direction: $dv_{p,i}/dt > 0$.

Numerical Method. In solving the full system (1)–(5), the gas flow field was first computed at each time layer, and then the equations of motion and heat transfer for particles [Eqs. (4) and (5)] were integrated using an implicit scheme.

The solution of Eqs. (1)–(3) was found by an implicit four-step finite-difference scheme of the type of a universal algorithm with splitting in terms of physical processes and spatial variables [9]. In constructing a high-resolution scheme for approximation of inviscid fluxes, we used a total variation diminishing (TVD) approach based on the van Leer flux-vector splitting [10]. A scheme with central differences was used to approximate viscous fluxes. The details and verification of the numerical algorithm are described in [11] by an example of a supersonic flow past a forward-facing step.

The size of the computational domain was chosen to reach an adequate resolution of the arising shock-wave structures of the flow. The computational grid had 150 to 200 nodes in the streamwise direction and 200 to 400 nodes in the transverse direction; the grid was refined toward the solid wall and in the vicinity of points with complicated geometry.

Discussion. Before computing the above-formulated problem, we should discuss the verification of the numerical method used on the basis of some test case. We consider the problem of particle lifting from a flat plate, initiated by a transient shock wave. The characteristics of lifting of a small particle of soot ($d_p = 30$ μm, $\rho_p = 2900$ kg/m^3, and $c_{\mathrm{S}} = 160$) in the flow field behind an SW with a Mach number $\mathrm{M}_{\mathrm{SW}} = 1.107$ were computed. The results are plotted in Fig. 2a, where they are compared with the results computed by a simplified model [2] and experimental data [5]. The computed results are seen to be consistent with the experimental data. The data in Fig. 2a are supplemented by the results in Fig. 2b, which shows the distributions of streamwise velocity of the gas in a certain cross section $x = \mathrm{const}$ behind the SW front. The computations underpredict the boundary-layer thickness (as compared with the self-similar solution) but overpredict the gradient of streamwise velocity inside the boundary layer. This ensures an approximately identical total action of the Saffman force on the particle in both cases.

Gas Flow in the Cavity. Transition of a shock wave with a Mach number $\mathrm{M}_{\mathrm{SW}} = 1.5$, 2.0, 3.0, and 4.0 over a cavity was computed. The cavity geometry could be varied: the taper angle $\alpha = 45^\circ$ and depth $H = 0.01$ m were constant, and the cavity length could be $L = 0.025$, 0.050, and 0.075 m, i.e., $L/H = 2.5$, 5.0, and 7.5, respectively.

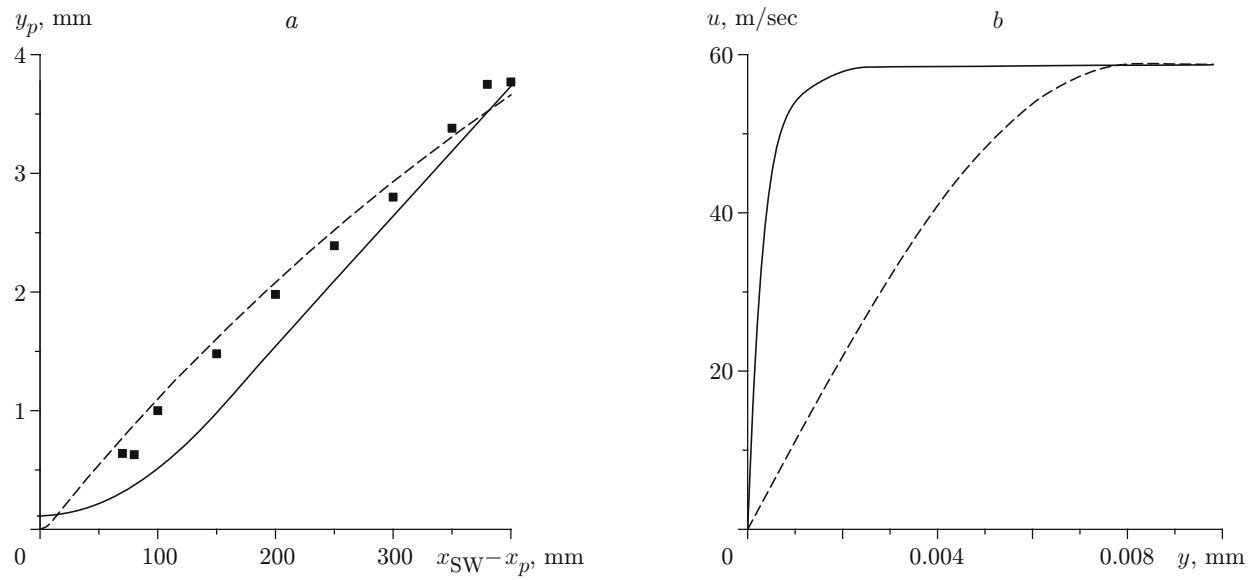

Fig. 2. Flow parameters behind the SW sliding along a solid wall ($M_{SW} = 1.107$): (a) height of soot-particle ($d_p = 30$ μm) lifting versus the particle position with respect to the SW front (the solid curve shows the results computed for $c_S = 160$, the dashed curve shows the results computed in [2], and the points are the experimental data of [5]); (b) streamwise velocity of the gas on a flat plate (the solid and dashed curves show the computed results and the self-similar solution, respectively).

Let us first consider the unsteady gas-dynamic pattern of the flow, which exerts a significant effect on particle lifting and dynamics. Depending on the SW intensity, the flow behind the SW front (in a motionless coordinate system) is either subsonic ($\tilde{M} \approx 0.6$ for $M_{SW} = 1.5$ and $\tilde{M} \approx 0.95$ for $M_{SW} = 2$, where $\tilde{M}$ is the flow Mach number behind the SW front) or supersonic ($\tilde{M} \approx 1.35$ for $M_{SW} = 3$ and $\tilde{M} \approx 1.54$ for $M_{SW} = 4$). Accordingly, the flow patterns in a cavity of unchanged geometry are different [12]. As the SW passes through the cavity, the SW front is incident onto the first inclined wall AB and becomes bent in the lower part, because the streamlines becomes curved along the surface. Then the SW moves to the lower wall of the cavity. At the corner point A, there arises a Prandtl–Meyer rarefaction wave, which interacts with the SW. Then the SW meets the second inclined wall, and an attached shock wave is formed in the vicinity of the compression corner C.

Figure 3 shows the streamlines for $\bar{t} = 1.131$ and $M_{SW} = 3$ (the bar is used to denote dimensionless quantities). It is seen that the flow structure in the cavity depends on L/H, which agrees with the experimental data of [12]. For $L/H = 2.5$, an open-type flow with one vortex in the entire region is formed in the cavity (Fig. 3a). For $L/H = 5$, a closed-type flow is formed. In this case, two separate vortex structures are formed in the compression corners B and C, and flow reattachment occurs in the lower part of the cavity (Fig. 3b). As the cavity length is increased, the dividing streamline moves further into the cavity volume, and a substantial mass of the gas penetrates into this region; the qualitative behavior of the streamlines remains unchanged.

Lifting and Dynamics of Particles. An analysis of the mathematical model shows that the governing parameters of the problem also include the initial particle coordinates and the SW intensity.

We considered the effect of the initial particle location on the characteristics of its lifting. For this purpose, we placed Plexiglas particles [$d_{p,0} = 225$ μm, $\rho_{22}^0 = 1200$ kg/m^3, and $c_{v,2} = 80$ J/(kg$\cdot$K)] to the bottom and top corner points A, B, C, and D and to points in the middle of the side walls and cavity bottom: particles 1 and 2 at the point A, particles 3 and 4 at the point in the middle of the left wall, particles 5 and 6 at the point B, particles 7 and 8 at the point in the middle of the cavity bottom, particles 9 and 10 at the point C, particles 11 and 12 at the point in the middle of the right wall, and particles 13 and 14 at the point D. The Saffman force coefficient for particles with odd numbers $(1, 3, \ldots, 13)$ was taken to be $c_S = 160$, which was obtained by the authors in [2]; the corresponding value for particles with even numbers $(2, 4, \ldots, 14)$ was $c_S = 32.2$ [5]. Note that lifting of particles of this size from a flat plate by the Saffman force is rather problematic, and the experimentally obtained lifting characteristics were attributed in [2] to the effect of aerodynamic interference acting on the particle.

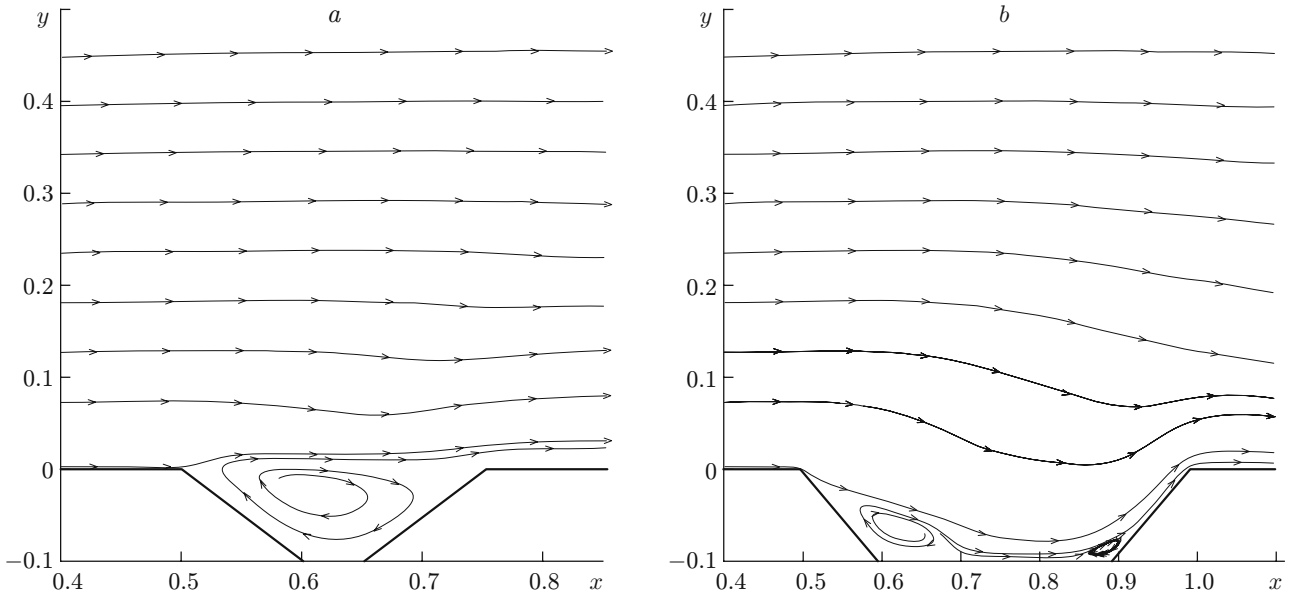

Fig. 3. Instantaneous streamlines for $\bar{t} = 1.131$, $\mathrm{M_{SW}} = 3$, and $L/H = 2.5$ (a) and 5 (b).

Figures 4a and 4b show the dimensionless dependence of the vertical coordinate of particles on time for a cavity of length $L/H = 5$ under the action of a shock wave with $\mathrm{M_{SW}} = 2$ ($u_* = 695$ m/sec and $t_* = 1.439 \cdot 10^{-4}$ sec). Obviously, particles affected by the Saffman force of greater intensity are lifted faster: the greatest lifting distance at the time $\bar{t} \approx 2.6$ is observed for particles 1, 7, 11, 13, and 14. These particles were initially located in the expansion corners (particles 1, 13, and 14), on the right wall (particle 11), and on the cavity bottom (particle 7). No noticeable lifting is observed for particles initially located on the left side wall of the cavity (particles 3 and 4): they are entrained to the cavity bottom by the gas flow (curves 3 and 4 in Fig. 4a). Particles located on the right side wall, where the flow is directed upward from the cavity bottom, are entrained by the gas flow upward along the surface; therefore, lifting of particles 11 and 12 is clearly visible (curves 11 and 12 in Fig. 4a). Particles initially located in the compression corners B and C are subjected to adverse gas-dynamic flow conditions for particle separation from the surface. This is especially pronounced in the left compression corner (curves 5 and 6 in Fig. 4b), where the particles become deposited onto the wall after insignificant lifting. Note that particle 8 is also deposited onto the wall.

We considered particle lifting from the cavity bottom in more detail. For this purpose, we observed the trajectories of additional particles (at $c_{\mathrm{S}} = 160$) located on the cavity bottom between particles 5, 7, and 9 (Fig. 4c). It follows from Fig. 4c that two segments can be distinguished on the cavity bottom ($\bar{x}_B = 0.6 \leqslant \bar{x} \leqslant \bar{x}_C = 0.9$): $I_- = [\bar{x}_B, \bar{x}_-]$ and $I_+ = (\bar{x}_-, \bar{x}_C]$. Particles being at rest in the segment I_- are separated from the wall, are lifted to a certain height (approximately five diameters), and finalize their motion (directed opposite to the external flow) by deposition onto the cavity bottom in the same segment (a rather small horizontal displacement of the particle from the corner B to the left wall of the cavity is neglected). Thus, the segment I_- can be treated as an "attracting set" for trajectories beginning in this segment. The range of possible finite motion of particles is bounded from above by an envelope (curve 1 in Fig. 4c) drawn through the apices of the trajectories observed and is bounded on the right by the vertical line $\bar{x} = \bar{x}_-$. Here the point $\bar{x}_-$ is determined as the beginning of the only trajectory that enters the corner point B. In this case, the trajectory is located higher than all possible trajectories beginning in the segment I_-.

Particles initially located in the segment I_+ have two options: they separate with moderate "overshooting" in the direction opposite to the external flow (the height of lifting of such particles is bounded by the envelope curve 2 in Fig. 4c) and "land" on the bottom (curves 3, 3′, and 3″) or on the left wall (curves 4 and 4′); otherwise, they separate and then are entrained into the central part of the cavity (curve 5). Therefore, it would be natural to add two more points in the segment I_+ ($\bar{x}_{+,1}$ and $\bar{x}_{+,2}$) dividing the intervals with different above-mentioned types of particle trajectories beginning in this segment.

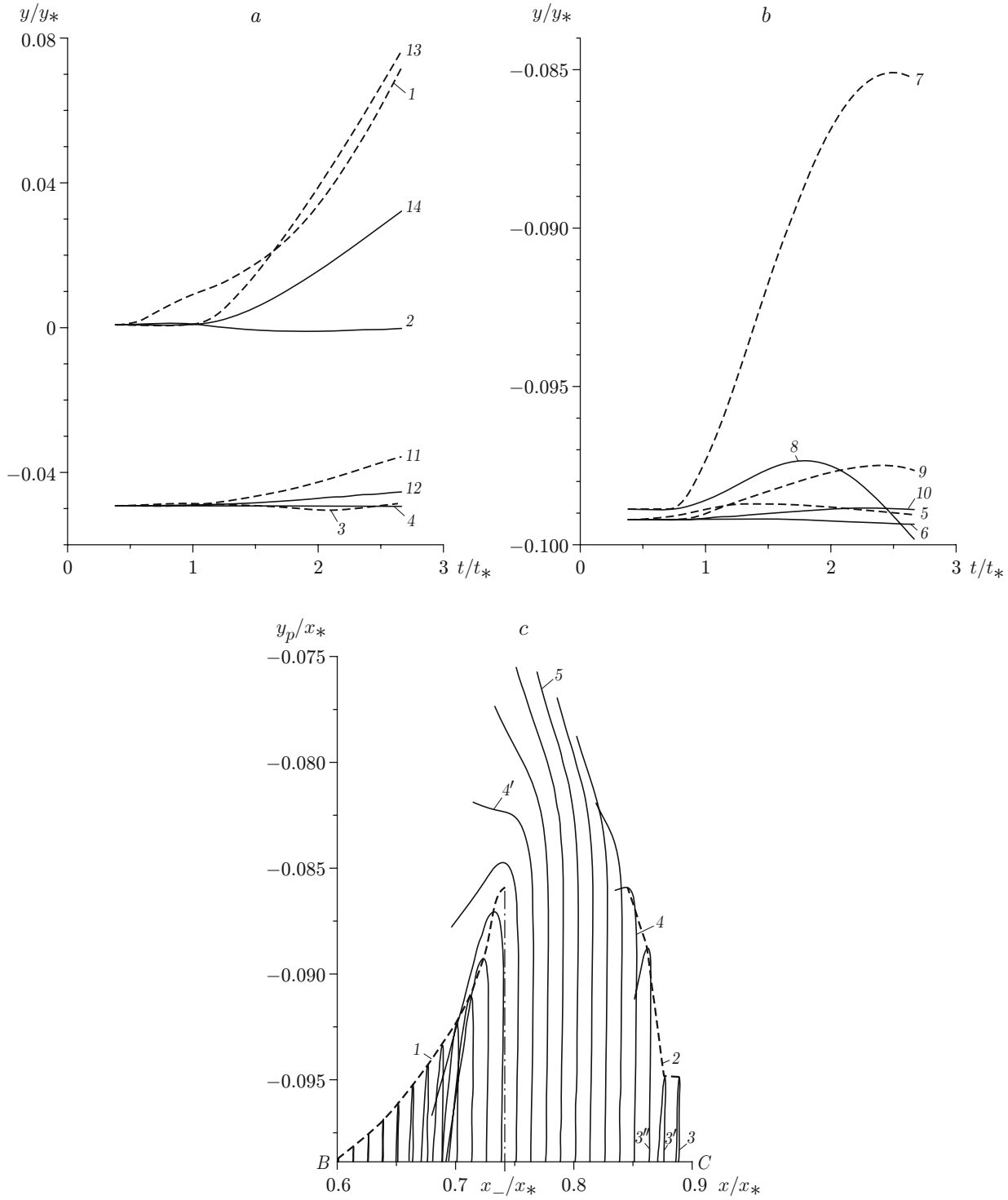

Fig. 4. Vertical coordinates of particles ($M_{SW} = 2$) versus lifting time from expansion corners and side walls of the cavity (a), from compression corners and cavity bottom (b) (1–14 are the particle numbers; the solid and dashed curves show the results for particles with even and odd numbers, respectively), and from the cavity bottom (c) (the dashed curves 1 and 2 are the envelopes of trajectory apices, the solid curves 3, 3′, 3″, 4, 4′, and 5 are the trajectories of individual particles with different initial positions, and the dot-and-dashed curve indicates the position of the limiting line $\bar{x} = \bar{x}_-$).

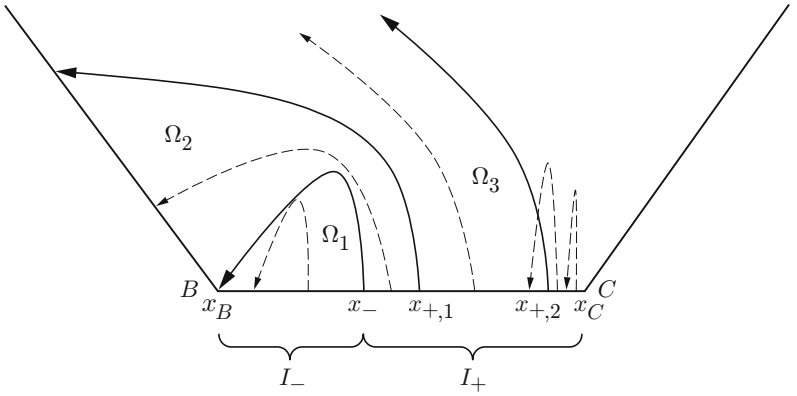

Fig. 5. Scheme of lifting and transportation of coarse particles from the cavity bottom: the solid curves are the limiting trajectories dividing the characteristic domains Ω_1, Ω_2, and Ω_3; the dashed curves are typical trajectories of individual particles.

TABLE 1

Time of Particle Separation ($\bar{t}_{\mathrm{lif},i}$) Versus the Particle Number (i) for $\mathrm{M_{SW}} = 2$

i	$\bar{t}_{\mathrm{lif},i}$	$\Delta\bar{t}_{\mathrm{lif},i}$	i	$\bar{t}_{\mathrm{lif},i}$	$\Delta\bar{t}_{\mathrm{lif},i}$
1	0.383	0	8	0.661	0.278
2	0.383	0	9	0.800	0.417
3	0.419	0.036	10	0.815	0.432
4	0.433	0.050	11	0.847	0.464
5	0.495	0.112	12	0.863	0.480
6	0.516	0.133	13	0.891	0.508
7	0.646	0.263	14	0.903	0.520

TABLE 2

Computed and Estimated Values of the Separation Delay $\Delta\bar{t}_{\mathrm{lif},i}$ for $\mathrm{M_{SW}} = 2$

i	$\Delta\bar{t}_{\mathrm{lif},i}$		δ, %
	Computation	Estimate	
3	0.036	0.05	28
5	0.112	0.10	11
7	0.263	0.25	5
9	0.417	0.40	4
11	0.464	0.45	3
13	0.508	0.50	1.6

It should be noted that disperse-phase particles located on the cavity bottom near the compression corners B and C are subjected to saltation, which allows motion of particles over the cavity bottom. The reason is that the particle settled down on the bottom can be lifted again and become deposited onto the walls. Thus, a relay-type mechanism of particle transportation from the vicinity of the compression corner C to the central part of the bottom with possible subsequent lifting to the external flow or deposition onto the side wall and aggregation of particles in the vicinity of the compression corner B can be expected.

Based on the results obtained, we can suggest a qualitative scheme of lifting of coarse particles from the cavity bottom (Fig. 5). The scheme contains the characteristic domains Ω_i (divided by the solid curves, which are the limiting trajectories) with different types of particle motion: all particle trajectories in the domain Ω_1 end in the segment I_-, all particle trajectories in the domain Ω_2 end on the left wall AB, and all particles from the non-closed domain Ω_3 are entrained into the external flow. The non-limiting trajectories of particles inside these domains are plotted by the dashed curves. More detailed information on particle lifting from the cavity bottom can be obtained by means of computations with a greater number of particles of different sizes and with greater values of t.

The data on the time of particle separation from the surface $\bar{t}_{\mathrm{lif},i}$ and the delay in separation of the ith particle, as compared to the first particle, $\Delta\bar{t}_{\mathrm{lif},i} = \bar{t}_{\mathrm{lif},i} - \bar{t}_{\mathrm{lif},1}$ are summarized in Table 1. It is seen that the dependence of $\bar{t}_{\mathrm{lif},i}$ on the particle number is monotonically increasing for both even and odd values of i, which is consistent with the direction of shock-wave propagation in the cavity. In this case, the SW front intersects particles 1 and 2 at the time $\bar{t}_{\mathrm{SW},1} = 0.381$, i.e., the delay in lifting of these particles is very small and amounts to $\bar{t}_{\mathrm{lif},i} - \bar{t}_{\mathrm{SW},1} = 0.002$.

We tried to justify the data on $\Delta\bar{t}_{\mathrm{lif},i}$ obtained for particles with odd numbers (for $c_{\mathrm{S}} = 160$), taking into account that the dimensionless SW velocity equals unity. The streamwise distance between particles 1 and 3 is 0.05. Hence, the separation delay for particle 3 (the delay in lifting is ignored), as compared with particle 1, is $\Delta\bar{t}_{\mathrm{lif},3} \approx 0.05/1 = 0.05$, which exceeds the computed value by $\delta = 28\%$. For subsequent particles, a farther distance

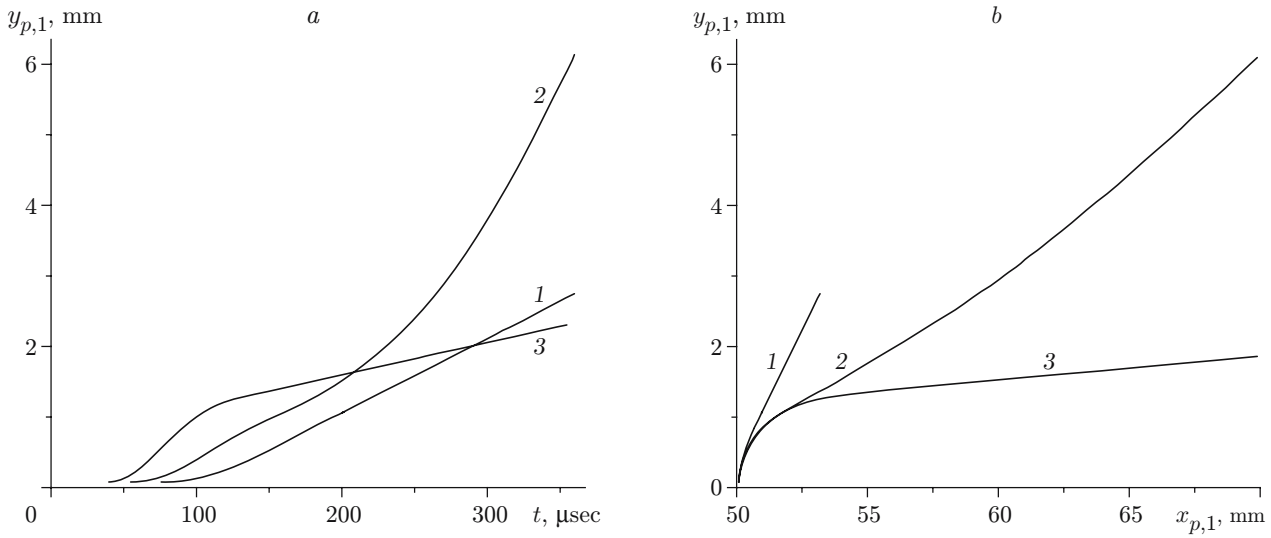

Fig. 6. Lifting height versus time (a) and possible trajectories (b) of particle 1 for different intensities of the transient SW: $M_{SW} = 1.5$ (1), 2 (2), and 3 (3).

of the particle improves the estimate accuracy (Table 2). Thus, for particles with elevated mobility in the boundary layer (high value of the Saffman force), which are remote from the left expansion corner and left wall of a cavity of moderate depth, the delay in lifting of the neighboring particles is determined by the time of SW arrival at the particle location, as in the case of particle lifting from a flat surface. Different lifting velocities of these particles are caused by the difference in parameters of the carrier-phase flow in the corresponding regions of the cavity.

We examined the influence of the SW Mach number on the lifting characteristics. Note that the dependence of the particle lifting height at a certain time on the SW Mach number is monotonic, except for lifting of particles located in the vicinity of the corner A.

Figure 6 shows the data characterizing lifting of particle 1 for different SW intensities. For higher SW intensities, particle lifting begins earlier, because a stronger shock wave reaches the particle faster (curve 3 in Fig. 6a). Before the time $t \approx 100$ μsec. curves 1–3 in Fig. 6a, which describe the vertical coordinate of the particle versus time, have a similar character. In a stronger SW ($M_{SW} = 3$), the particle acquires a greater vertical velocity $v_{p,1}$. At $t > 100$ μsec, its value decreases for $M_{SW} = 3$. As a result, the lifting height reached during 360 μsec is smaller than that for $M_{SW} = 1.5$. This behavior of the particle in the flow behind the SW with $M_{SW} = 3$ can be attributed to stronger (as compared with other cases) entrainment of the particle by the flow in the horizontal direction. At $t < 100$ μsec ($x_{p,1} < 60$ mm), the particle trajectory for $M_{SW} = 3$ almost coincides with the trajectory for $M_{SW} = 2$ (curves 2 and 3 in Fig. 6a).

Conclusions. Characteristics of the flow arising when a planar shock wave passes through a cavity of moderate depth have been considered. The separated character of the flow in the cavity (thick shear layers) favors lifting of rather coarse particles from the walls, which is rather difficult in the flat-plate case.

Lifting of particles from the cavity walls is substantially affected by their initial position and by SW intensity. Particles initially located in the vicinity of expansion corners, on the cavity bottom, and on the right wall experience lifting to the greatest height. The dependences of the particle lifting height at a certain time on the initial streamwise coordinate and SW Mach number are nonmonotonic.

Particles can be redistributed over the cavity bottom in the direction opposite to the external flow owing to the saltation mechanism. There are two qualitatively different segments on the cavity bottom: in the first segment, particles are transported toward the central part of the cavity and then are lifted and brought out from the cavity; in the second segment, stable aggregation of particles near the left compression corner occurs.

For particles remote from the expansion corner, the lifting delay (as compared with that for the neighboring particle) is determined by the time of arrival of the shock wave at the particle location, similar to the case of lifting from a flat surface.

REFERENCES

1. A. V. Fedorov, "Mixing in wave processes propagating in gas mixtures (Review)," *Combust., Expl., Shock Waves*, **40**, No. 1, 17–31 (2004).
2. Yu. A. Gosteev and A. V. Fedorov, "Calculation of dust lifting by a transient shock wave," *Combust., Expl., Shock Waves*, **38**, No. 3, 322–326 (2002).
3. B. Y. Wang, Q. S. Wu, C. Wang, et al., "Shock wave diffraction by a square cavity filled with dusty gas," *Shock Waves*, **11**, No. 1, 7–14 (2001).
4. T. R. Amanbaev, "Lifting of disperse particles from a cavity behind the front of an unsteady shock wave with a triangular velocity profile," *J. Appl. Mech. Tech. Phys.*, **44**, No. 5, 634–639 (2003).
5. W. Merzkirch and K. Bracht, "The erosion of dust by a shock wave in air: Initial stages with laminar flow," *Int. J. Multiphase Flow*, **4**, 89–95 (1978).
6. V. F. Volkov, A. V. Fedorov, and V. M. Fomin, "Problem of the interaction between a supersonic flow and a cloud of particles," *J. Appl. Mech. Tech. Phys.*, **35**, No. 6, 832–836 (1994).
7. Yu. A. Gosteev and A. V. Fedorov, "Mathematical simulation of lifting and ignition of particles of coal deposits," *Combust., Expl., Shock Waves*, **39**, No. 2, 177–184 (2003).
8. D. C. Wilcox, *Turbulence Modeling for CFD*, DCW Ind. Inc., La Caňada, California (1993).
9. V. M. Kovenya and N. N. Yanenko, *Splitting Method in Gas-Dynamic Problems* [in Russian], Nauka, Novosibirsk (1981).
10. B. van Leer, "Flux-vector splitting for the Euler equations," *Lecture Notes Phys.*, **218**, 566–570 (1985).
11. I. A. Bedarev and N. N. Fedorova, "Investigation of factors affecting the quality of prediction of turbulent separated flows," *Vychisl. Tekhnol.*, **4**, No. 1, 14–33 (1999).
12. P. Chang, *Separation of Flow*, Pergamon Press, Oxford (1970).